MODELING, IDENTIFICATION AND CONTROL, 1992, VOL. 13, NO. 1, 51–63
doi:10.4173/mic.1992.1.5

The realization of a permanent magnet synchronous motor drive with flux weakening, digital current control and voltage vector modulation

LARS NORUM†, ALF KÅRE ÅDNANES‡,
WALDEMAR SULKOWSKI† and LARS ARNE AGA†

Keyword index: *PMSM drives, flux weakening, digital control, microcontroller.*

This paper presents the realization and performance of a fully digital permanent magnet synchronous motor drive. A new control algorithm gives maximum torque to current ratio in both the constant torque region and in flux weakening. Inner loop current control and vector modulation with short calculation time are obtained by the use of look-up tables. The controller is implemented in a singleboard control computer for power electronics systems, which is based on a 16 bit microcontroller.

1. Introduction

Because of high efficiency, combined with possible compact designs, permanent magnet excited AC motors are interesting in battery fed drives, as in electric traction and remotely operated vehicles. In these applications, the torque requirement is usually high for low speeds, but allows decreased torque at higher speeds, i.e. requirements which typically are met by field weakening in traditional motor drives. The salient pole permanent magnet synchronous motor (PMSM) is an interesting alternative for drives where a torque characteristic with flux weakening is requested (Jahns 1987, Bose 1987 and Ådnanes 1991). A new controller with flux weakening was previously presented (Ådnanes and Undeland 1991). This controller ensures maximum torque to the current ratio in both the constant torque region and in flux weakening.

A digital current controller and voltage modulation can only give high bandwidth current control when the execution time is short, typically $<250\,\mu$s. In reported digital current controllers, either fast signal processors or ASICs have been used to obtain satisfactory calculation speed. These solutions give additional complexity in controller hardware and substantial software challenges. However, the performance of single chip microcontrollers is improving rapidly. This paper presents a PMSM drive with a fully digital regulator implemented in a microcontroller with on-chip peripherals without additional processing circuits.

It was necessary to develop a simple, fast modulation algorithm, suitable for digital implementation for this application. Here, the voltage selection (VVS) and the voltage averaging (VA) modulation methods (Pfaff *et al.* 1982) are of particular interest. VVS is preferable for fast calculation. However, the current ripples are much larger than with VA. In the present work, VA and VVS techniques are combined to make a fast current control and modulation algorithm.

Received 18 December 1991.

† Department of Electrical Engineering, and Computer Science, The Norwegian Institute of Technology, N-7034 Trondheim, Norway.

‡ ABB Corporate Research, PO Box 90, N–1361 Billingstad, Norway.

The control algorithms have been tested on an experimental 2·8 kW PMSM drive. The applied control strategies are presented, but the paper mostly focuses on the realization of the digital controller and its performance. The drive is schematically illustrated in Fig. 1.

2. Control principle

2.1. *A control algorithm with flux weakening*

The vector diagram for a salient pole PMSM at stationary is presented in Fig. 2 in a rotor oriented *dq*-frame. The direct axis is aligned with the vector which represents the flux linkages from the magnet, Ψ_m. In contrast to the electrically excited synchronous motors, the quadrature axis reactance x_q is larger than the direct axis reactance x_d. For a constant current vector amplitude to torque is maximum at a torque angle β greater than 90°. A trajectory for maximum torque to current ratio, the optimum current trajectory, is located in the second quadrant of the *dq*-frame as shown in Fig. 3 for positive torque (motoring), and in the third quadrant for negative torque (breaking) (Ådnanes 1991).

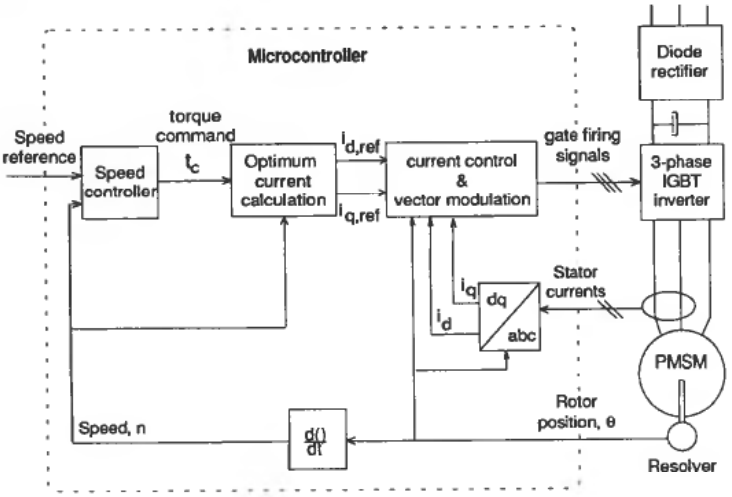

Figure 1. A fully digital PMSM drive.

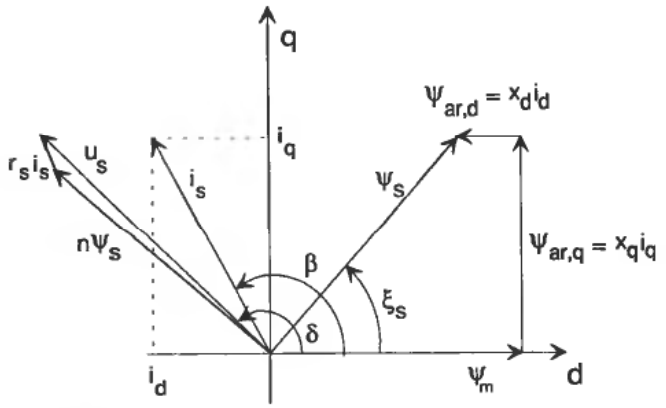

Figure 2. Vector diagram for salient pole PMSM (per unit).

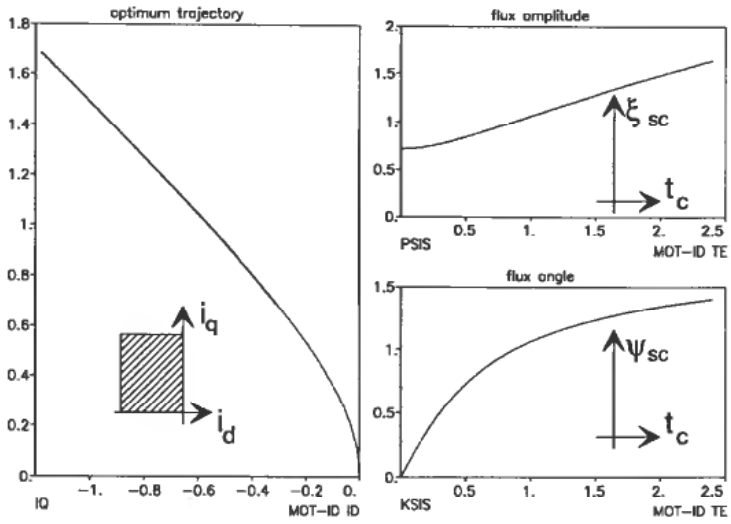

Figure 3. The optimum current trajectory (left) and the corresponding stator flux amplitude (upper right) and angle (lower right) for the salient pole PMSM described in the appendix.

The optimum current trajectory can be expressed by the stator flux amplitude Ψ_s and its angle ξ_s, as shown in Fig. 3 for positive torque. For negative torque, Ψ_s remains unchanged but ξ_s is negative due to symmetry. With knowledge of motor parameters, these functions can be precalculated and stored in a look-up table as the commanded flux amplitude Ψ_{sc} and angle ξ_{sc} which correspond to a torque command t_c.

Once the requested stator flux linkages have been calculated, current references in the direct and quadrature axes are derived via the armature reaction components $\Psi_{ar,d}$ and $\Psi_{ar,q}$

$$i_{d,\mathrm{ref}}=\frac{\Psi_{ar,d}}{x_d}=\frac{\Psi_{sc}\cdot\cos\xi_{sc}-\Psi_m}{x_d} \tag{1}$$

$$i_{q,\mathrm{ref}}=\frac{\Psi_{ar,q}}{x_q}=\frac{\Psi_{sc}\cdot\sin\xi_{sc}}{x_q}. \tag{2}$$

By choosing the stator flux as an indirect control variable, flux limiting is obtained by restricting the flux amplitude command Ψ_{sc} to ensure that the current space vector is inside the voltage limiting boundary at any speed. If the resistive voltage drop $r_s i_s$ is neglected, the stator voltage is $u_s=n\cdot\Psi_s$ where n is the rotor speed in per unit. If 1·0 per unit voltage corresponds to the maximum inverter voltage, then

$$\Psi_{sc,\max}=\frac{1}{n} \tag{3}$$

The maximum speed gives the lower limit:

$$\Psi_{sc,\min}=\frac{1}{n_{\max}}. \tag{4}$$

For a fixed flux, the maximum possible torque is obtained with a speed dependent flux angle somewhat greater than 90°. For simplicity and with less practical importance, the flux angle limits are chosen to be constant:

$$\xi_{sc,\max}=90° \tag{5}$$

$$\xi_{sc,\min}=-90°. \tag{6}$$

The torque and flux control algorithm scheduled in Fig. 4 forces the current references to follow the optimum trajectory below flux weakening, and the voltage limiting boundary in flux weakening. Optimum control is thus accomplished at all speeds.

2.2. *Inner loop current control with vector modulation*

The current reference components i_{dref} and i_{qref} are inputs from the outer loop to the current controller. The measured currents are transformed to the synchronous reference frame. The block diagram of the Voltage Space Vector Current Regulator is shown in Fig. 5.

By application of a synchronous PI controller in both axes the cross-coupling components in steady-state are compensated without additional calculation (Rowan and Kerkman 1986). The resulting signals u_{dc} and u_{qc} are references to the voltage space vector modulator. Precalculated look-up tables are used, one for the vector modulus and one for the angle, for fast Cartesian to polar coordinate transformation. The tables have limited size due to memory limitations in the experimental set-up. Larger tables would not have influenced the execution time. The digital values u_{dc} and u_{qc} are addresses which point to these tables. The accuracy of u_{dc} and u_{qc} are better than the resolution of the tables. In the low speed region where the voltage vector amplitude is low, the accuracy of angle calculation is improved by the multiplication of both addresses by a common constant scaling factor. The polar space vector in stator coordinates is used to select voltage vectors and a proper time sequence.

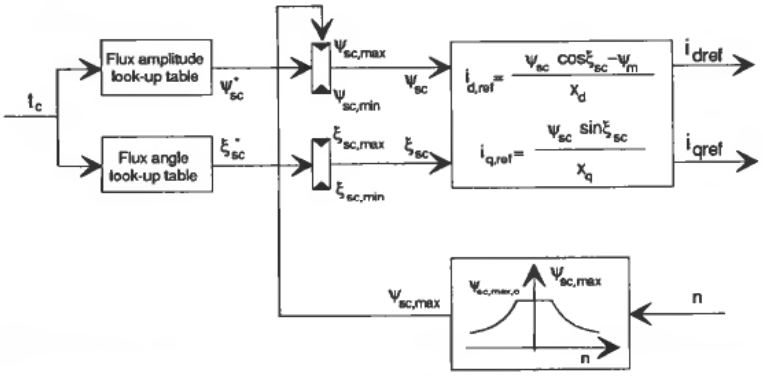

Figure 4. The algorithm for optimum current calculation with flux weakening for a salient pole PMSM.

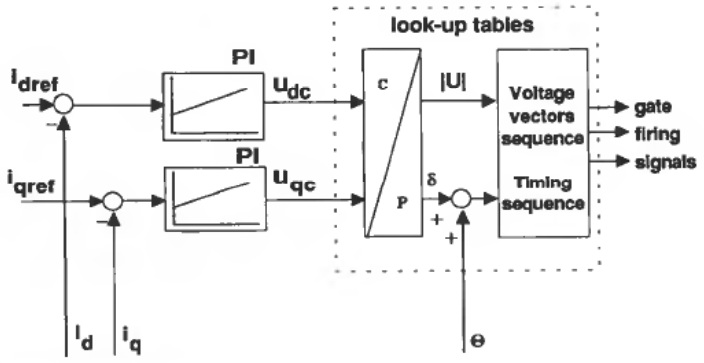

Figure 5. The block diagram of the Voltage Space Vector Current Regulator for PWM-VSI.

The Voltage Space Vector Averaging (VA) method is used to apply a selected reference voltage vector to the load. Any reference voltage vector which is located between two adjacent active vectors can be expressed by their weighted combination and passive zero vectors as shown in Fig. 6 (Pollmann 1986, Pfaff *et al.* 1982):

$$\boldsymbol{u}_c = \begin{bmatrix} u_{dc} \\ u_{qc} \end{bmatrix} = x \cdot \boldsymbol{u}_L + y \cdot \boldsymbol{u}_R. \tag{7}$$

The requested voltage $\boldsymbol{u}_c$ is in average obtained if the active vectors are applied with time sequences as shown in Fig. 6(*b*), where:

$$x = \frac{T_R}{T_s} \quad \text{and} \quad y = \frac{T_L}{T_s}. \tag{8}$$

T_R is the time duration for the right neighbouring vector $\boldsymbol{u}_R$, T_L is the time duration for the left vector $\boldsymbol{u}_L$, and T_s is the sampling time. The zero vectors are applied for the remaining time of the sampling period:

$$T_0 = T_s - T_R - T_L. \tag{9}$$

For minimum number of switching, the inverter should change state by switching in one inverter leg only. The sequence of the active vectors must then be given by the last applied zero vector. The time sequences alternate every other sampling period is shown in Fig. 6. For example, if the left active vector is number 1 and the right is number 2, the switching sequence over two sampling periods becomes 0-1-2-7-1-0. The output voltage is then in agreement with the Pulse Polarity Consistency Rule (Abbondanti *et al.* 1975) which states that the line to line voltage should be monopolar during each half of the fundamental period.

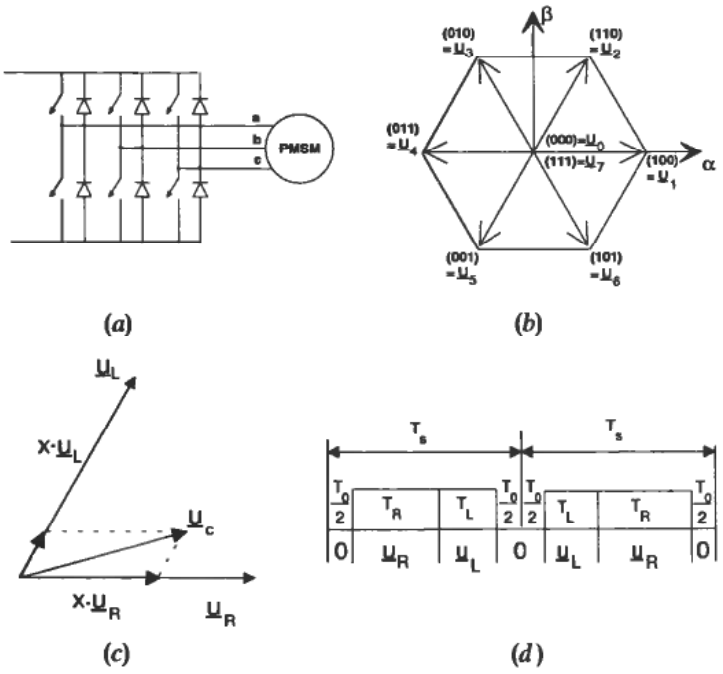

Figure 6. The principles of space vector weighted averaging method: (*a*) Three-phase inverter, (*b*) the six active and two zero voltage vectors, (*c*) voltage diagram, (*d*) time sequence.

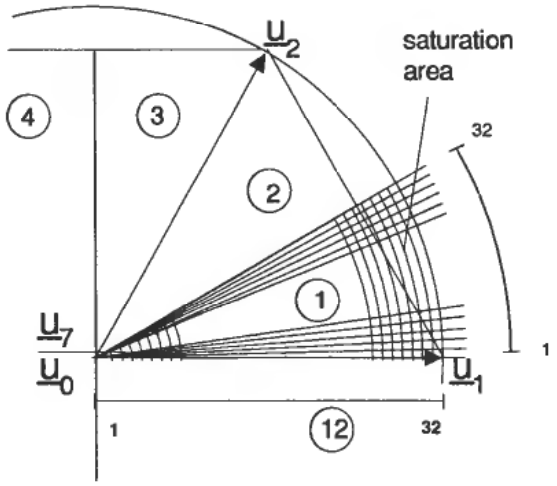

Figure 7. The principle of voltage vector plane division and time sequence discretization for VA.

The complex plane is divided into 12 sectors with assigned voltage sequences attributes. Using symmetry it is sufficient to describe precise timing sequences for only one of the twelve sectors. The same timing sequences are applied in the other sectors with different voltage vectors. The principles of sector division and time sequence attribution are shown in Figs. 7 and 6(*b*).

The VA method allows precise sinusoidal modulation and utilizes the maximum voltage vector hexagonal region. The physical limitations of the voltage region are defined by time sequences in look-up tables. To avoid vector displacement error in the saturation area shown in Fig. 7, the current hexagonal boundary.

3. Implementation of an experimental drive

3.1. *Hardware description*

An experimental PMSM drive with a commercial 2·8 kW salient pole motor and fully digital current controller has been tested. The motor data listed in the appendix are given by the manufacturer. The motor is supplied from a three-phase inverter with IGBT switches.

The controller is implemented in a single-board power electronics control computer. The PECC is based on an INTEL 80C196KC microcontroller. This single-chip controller has six high speed output (HSO) lines and 8 input channels for the A/D converter. The time instants for HSO actions are stored in the content addressable memory (CAM). The HSO unit and the interrupt at A/D conversion are utilized to obtain a fast algorithm for the most time critical tasks. The 32kB RAM and 32kB ROM give sufficient space for the programs, look-up tables and also logging of control variables and measurements. User communication and presentation of monitored data are taken care of by a PC connected to the RS232 port. Figure 8 gives an overview of the hardware. For simplicity, only the functions which are necessary for this drive are shown, and the control signals are omitted.

A resolver on the shaft provides the rotor position. Resolver to digital (R/D) conversion is performed by an AD2S80KD from Analog Devices. The maximum speed limits the resolution of position to 12 bits. The digital output is read into the microcontroller in two bytes.

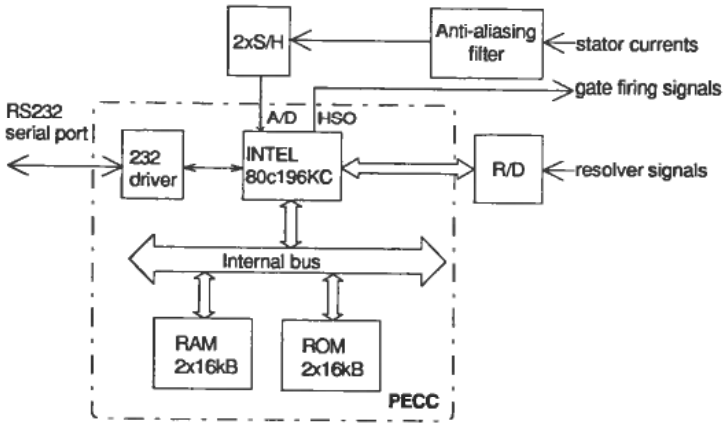

Figure 8. Block diagram of the controller hardware.

Additional sample and hold (S/H) circuits ensure simultaneous sampling of the measured currents. The currents are measured with LEM transfoshunts in two phases only, since no zero sequence currents are present. The content of switching ripple in the currents make it necessary to filter the measurements to avoid aliasing, since sampling is not synchronized. Time delays in the current control loop cause errors in torque control at higher speeds, thus the phase shift caused by the filter should be minimized. A lowpass filter with 1kHz bandwidth reduced the switching ripple to less than 1% of rated current, which was considered acceptable.

For practical considerations, the controller circuits have been located on three standard Europe cards. However, the necessary circuits cover an area smaller than the size of a double Europe card.

4. Software description

A small operating system PECCROS is developed and used for PECC applications. PECCROS acts as the user interface by interaction with a PC terminal program PECCTerm. Communication tasks are executed when other activities are idle. The controller is divided in two separate tasks:

1. The outer loop is started every millisecond. It performs speed regulation and calculates optimum currents in the *dq* frame.
2. The current control loop is initiated when the A/D conversion is completed. The HSO starts A/D conversion every 200 μs which gives a 5 kHz sampling frequency.

The two tasks exchange information by common variables in RAM. The outer control loop reads the time stamped rotor position from the inner loop, and writes current references.

Outer control loop. The speed is estimated by differentiation of the rotor position. An IIR-filter reduces the discretization noise. The speed controller output is used as the torque command, and limited to 2 per unit. The flux amplitude and angle as functions of torque command are stored in two look-up tables with 512 words each. The sine/cosine functions of the optimum current calculation, eqns (1, 2), are stored in a table with 512 steps per 360 degrees.

Inner control loop. The current control loop is the most time critical and time consuming task in this application and it has the highest priority. The time delay

between measurements and controller output is minimized. The timing relations of the current controller are shown in Fig. 9.

While the A/D conversion of phase B current is carried out, the rotor position is read and the HSO CAM registers are loaded in order to prepare the next sampling interval. The measured currents are transformed to the *dq*-frame by applying the same sine and cosine functions as used in the optimum current calculation.

The PI current controllers consist of shift and add instructions, in order to reduce the execution time. Thus the proportional gain and integration time of the controller can only be changed by factors of two. The output from the current controller are the voltage commands u_{dc} and u_{qc} in the *dq*-frame, see Fig. 10. Transformation to polar coordinates is obtained by look-up in the 32×32 word table. The amplitude u_{sc} and angle in the stator frame are used as a pointer to a table which gives the sector number (1 through 12) and a pointer to the corresponding switching time sequence. This table is defined for the upper half plane only by the use of symmetry. It reduces the table size by a factor of two at the expense of one additional test. The chosen resolution for voltage vector angle (128 steps per 360°) and amplitude (32 steps) results in a table with 2 K words.

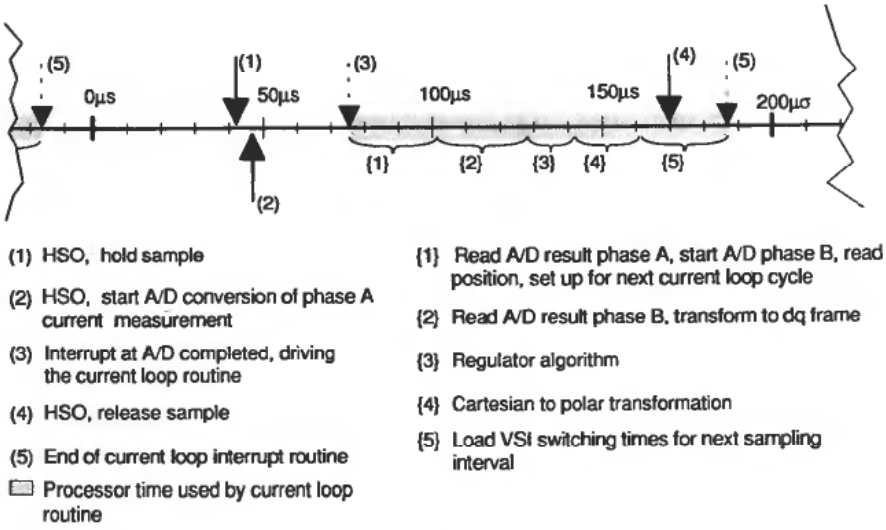

Figure 9. Timing relations in the current loop.

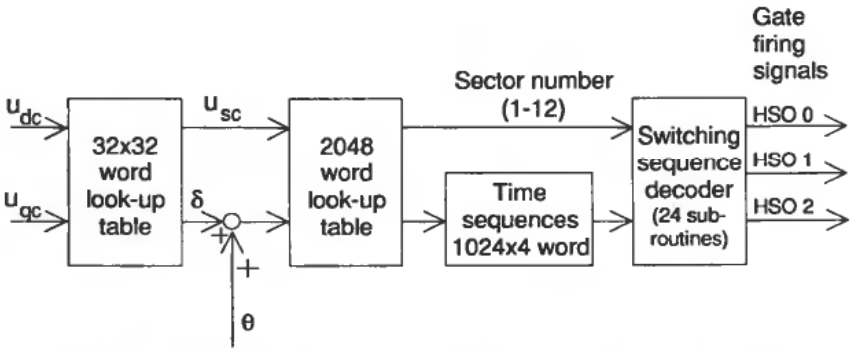

Figure 10. Realization of a vector modulator with look-up tables.

The voltage plane is divided in 12 sectors of 30°. The switching time sequences are described in one sector only. The active vectors are given by the sector number. The time duration of the active vectors is read from the time sequence table (4 K words). The last applied zero vector determines the switching order. Hence there are 24 possible switching sequences, each is allocated one subroutine which preloads the HSO CAM. The HSO unit then activates the transistor gate signals without further CPU interaction.

5. Experimental

5.1. *Performance of the current controller*

The performance of the current controller can be described by the response to a step change in current reference. The rise time and the overshoot of the current response are trade-offs when tuning the parameters of the current controller. In one servo drive for robot applications the specifications were a current rise time of less than 1 ms and maximum 30% overshoot with a small step change in the current reference at standstill. These specifications were used as objectives for the current controller.

Current responses have been tested with the rotor position locked at zero degrees. The measured currents were logged in two phases by a digital storage recorder. Using the built-in mathematical functions of the recorder, the currents were transformed to stationary orthogonal coordinates which coincided with the *dq*-frame. Figure 11 shows the response in both axes to a step change in the *q*-axis current reference of one per unit. Figure 12 shows the *d*-axis current after a step change in the reference of 0·5 per unit. The current controllers were not saturated in these tests. The rise time is 800 μs in both axes with an overshoot of 35% in the quadrature axis 5% in the direct axis. The control is not fully decoupled even at standstill. This is due to the limited resolution of the tables of the vector modulator. Since only a limited number of voltages can be applied, there are voltage components in the direct axis which disturbs the current. Figure 13 shows the current components as logged from the microcontroller. These show good agreement with the measured currents in Fig. 11.

In Fig. 14, the motor was initially in steady state with low load at about 2000 rpm. The figure shows the logged response to a step change in the *q*-axis current reference of

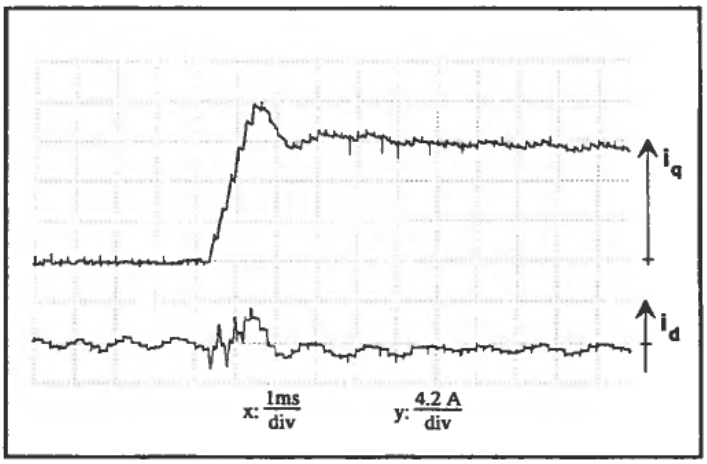

Figure 11. The measured current response to a step change in the quadrature axis current reference with locked rotor.

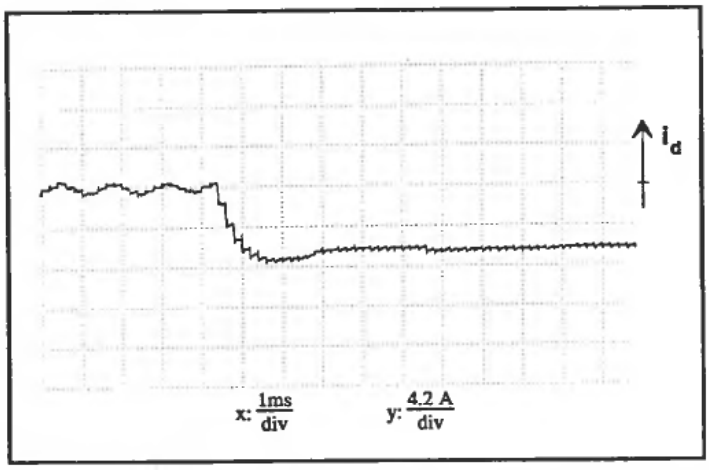

Figure 12. The measured current response to a step change in the direct axis current reference with locked rotor.

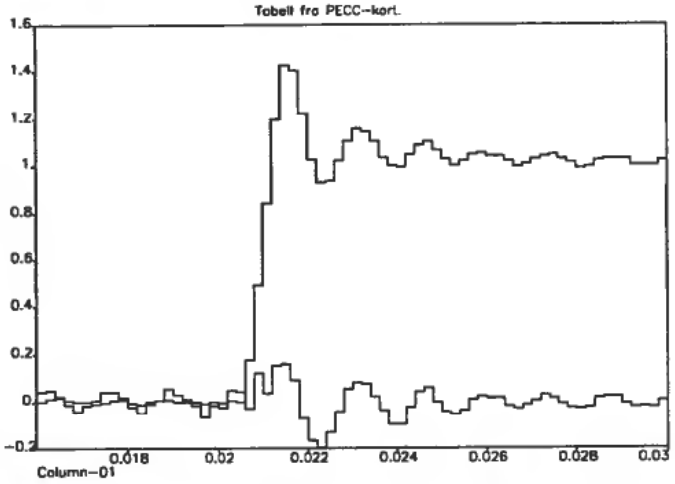

Figure 13. The logged current response to a step change in the quadrature axis current reference with locked rotor.

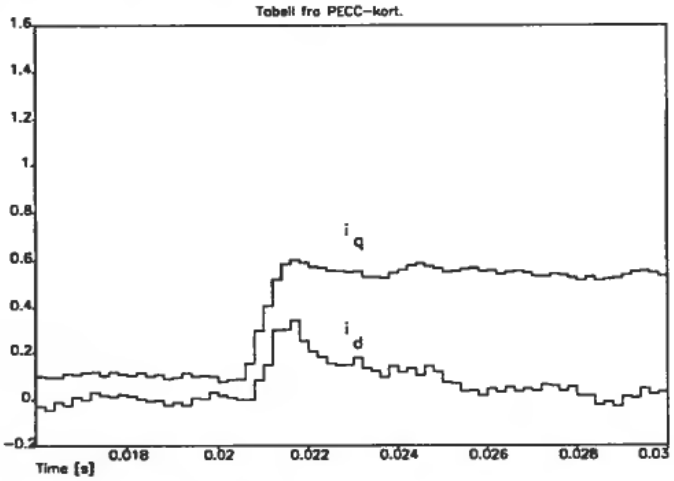

Figure 14. The logged current response to a step change in the quadrature axis current reference, n = 2000 rpm.

0·5 per unit. The speed dependent cross coupling in the motor is compensated by the integration of the current controller only. The stationary performance is good with a PI controller, but the transient disturbance at high speed is considerable.

5.2. *Speed control*

A closed speed loop regulator as shown in Fig. 1 was implemented for the purpose of testing the flux weakening operation. The no-load DC link voltage was reduced to 120 V, thus flux weakening algorithm could be tested without exceeding the maximum speed for the motor and load. In the results shown, the load is purely inertial.

Figure 15 presents a speed reversal from −3000 rpm to 3000 rpm. The curves are logged by the microcontroller with an interval of 10 ms. Currents are scaled with rated values as base, and base speed is chosen equal 1200 rpm. The logical variable 'flux weakening' detects when the flux command is saturated.

The measurements show a good accuracy in the current control, except at high speed and large torque. The reason is that the current controllers are slightly saturated with this base speed. It must be noted that the DC link voltage was uncontrolled, and varied substantially with the load.

The relative large peak current in the direct axis current after the step change in speed reference is mainly due to the cross coupling effects described earlier.

6. Conclusions

The realization of a fully digital PMSM drive with flux weakening and vector modulation has been presented. The controller is implemented in a microcontroller

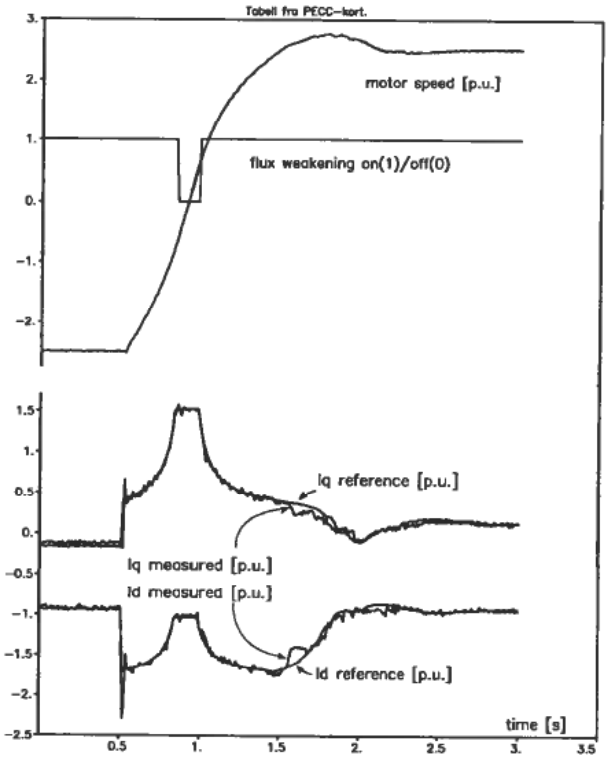

Figure 15. Measurements of a speed reversal from −3000 to +3000 (2·5 p.u.) rpm with inertial load.

based single-board computer card. To obtain fast execution time and high current loop bandwidth, transformations and switching time sequences for vector modulation were stored in look-up tables. With this solution, a 5 kHz sampling frequency was obtained for the current control loop. The current rise time was measured to 800 μs with an overshoot approximately 35% in the quadrature axis and 5% in the direct axis at standstill. Some cross coupling in the two axes was observed and more effort to reduce this has to be made.

The applied optimum current calculation algorithm gives a maximum torque to current ratio in the constant torque region as well as in flux weakening. The algorithm simplifies the calculation of the currents' phase advance in flux weakening. This was done in an outer loop which was calculated every millisecond. Tests with speed control have shown the validity of the control principle in a large speed range.

The development of high performance single chip microcontrollers is already at a level where fully digital controllers for PMSM drives are within reach without the need of additional processing circuits. Fully digital solutions have become a serious competitor to hybrid controllers.

Acknowledgments

The present work was partially a study for the degree of Doktor Ingeniør which was financed by the Norwegian Council for Scientific and Industrial Research (NTNF) through the Program for Robotic Research at the Norwegian Institute of Technology. NTNF is also acknowledged for W. Sulkowski's research fellowship which made his contributions to this work possible.

References

Abbondanti, A., Zubek, J., and Norby, C. J. (1975). Pulsewidth modulated inverter drives with improved modulation. *IEEE Trans. Ind. Appl.* **11,** 695–703.

Ådnanes, A. K. (1991). Torque analysis of permanent magnet synchronous motors. *Conf. rec. PESC*, Boston, USA, pp. 695–701.

Ådnanes, A. K., and Undeland, T. M. (1991). Optimum torque performance in PMSM drives above rated speed. *Conf. Proc. IEEE IAS annual meeting*, Dearborn, USA.

Bose, B. K. (1987). A high performance inverter-fed drive system of an interior permanent magnet synchronous motor. *Conf. Proc. IEEE IAS annual meeting*, Atlanta, USA, pp. 269–76.

Industrial Drives. B-206 Technical Data Publication. *Industrial Drives*, 201 Rock Road, Radford Virginia 24141.

Jahns, T. M. (1987). Flux weakening regime operation of an interior permanent-magnet synchronous motor drive. *IEEE Trans. Ind. Appl.*, **23,** 681–89.

Norum, L. (1986). Microprocessor applications in power electronics. *Dissertation*, (The Norwegian Institute of Technology).

Pfaff, G., Weschta, A., and Wick, A. (1982). Design and experimental results of a brushless ac servo-drive. *Conf. rec. IEEE IAS annual meeting*, pp. 692–97.

Pollmann, A. J. (1986). Software pulsewidth modulation for μP control of AC drives. *IEEE Trans. Ind. Appl.*, **22,** 691–696.

Rowan, T. M., and Kerkman, R. J. (1986). A new synchronous current regulator and analysis of current-regulated PWM inverters. *IEEE Trans. Ind. Appl.*, **22,** 678–690.

Appendices

Motor data

Manufacturer Industrial Drives		Model B-206-C
Rated current (rms)	I_{rated}	10 A
Rated voltage (rms, 1–1)	U_{rated}	250 V
Rated torque	T_{rated}	6·83 Nm
Rated speed	n_{rated}	4900 rpm
Direct axis inductance	L_d	5·33 mH
Quadrature axis inductance	L_q	13·8 mH
Back *emf* (rms 1–1)	K_E	37·7 V/krpm
Moment of inertia	J	$2{\cdot}512 \times 10^{-4}$ kgm^2